Electronic Supplementary Material (ESI) for Analyst.

Electronics Supporting Information (ESI)

Optomicrofluidic device for detection and isolation of drop encapsulated target cells in single-cell format

R. Gaikwad, A. K. Sen*

Department of Mechanical Engineering, Indian Institute of Technology Madras, Chennai-600036, India.
*Author to whom correspondence should be addressed. Email: ashis@iitm.ac.in

S1: Acquisition and post-processing of optical signals

The FSC, SSC and FL signals are analysed to obtain the height (intensity) and width (time duration) of the signals which are further utilised to generate scatter plots. The acquired data is further processed using a python program to eliminate the high frequency and random noise signals using the moving average algorithm. Python program is used to process the data for the various signals and generate the scatter plots. LABVIEW programs are also utilised to synchronise the supporting electronics used for droplet sorting. The program acquires and stores data from the NI-DAQ system and SPCM module. Along with the APD and PD data, SPCM data is continuously analysed (once every 1.0 ms) for its photon count and compared with a threshold value. If the acquired photon count is greater than the threshold value, then the Labview program communicates with the Arduino board to switch the original signal to a 'low' or 'high' signal, which further actuates the relay. In positive sorting, a 'high' signal is continuously written on a digital output pin of an Arduino board and the electrodes are continuously energised until the maximum photon count crosses a threshold value. At this point, a 'low' signal is written to de-energise the electrodes so the droplets containing target cells do not get coalesced and collected at the outlet 1. Similarly, in negative sorting, a 'low' signal is continuously written on a digital output pin of an Arduino board and the electrodes are de-energised until the maximum photon count crosses the threshold value. At this point, a 'high' signal is written to de-energise the electrodes so the droplets containing target cells/particles get coalesced and the particle/cells are collected at the outlet 2. The signal to the relay (based on the optical signal received) for deactivation of the electrode in case of positive sorting (or activation in case of negative sorting) is triggered some time (~3ms) before a target particle/cell arrives at the electrodes, which is attributed to the response time of the intermediate electronics.

S2: Particle focusing and drop encapsulation

Focusing of particles of 15 µm size present in an aqueous sample at a concentration 3.6×10^4 per ml and flow rate 1 µl/min using a mixture of DI water+glycerol (23% wt/wt) as sheath fluid at flow rate 7 µl/min toward one of the channel walls in the focusing region is presented in Fig. S1a (see video S1). The variation of the width of the focused stream w_f with the ratio of sheath to sample flow rates, $r = (Q_{sh}/Q_s)$ is shown in Fig. S1b. The spacing between the two adjacent particles in the focused region g_2 was studied by varying the sample concentration c_s (which affects the average spacing between the particles before focusing, g_1) and the results are presented in Fig. S1c. In a flow-focusing junction, three different regimes, namely squeezing, dripping and jetting, can be used for generating droplets[1] (Fig. S2a). A comparison of sizes of particle/cell encapsulating and empty droplets with continuous to discrete phase flow rate ratio r_f is shown in Fig. S2b. The separation distance between the droplets (i.e. droplet frequency) can also be controlled by varying the continuous to droplet phase flow rate ratio, as shown in Fig. S2c. The frequency of arrival of particles needs to match the frequency of droplet generation to ensure that each of the droplets encapsulates one particle only. If the frequency of arrival of particles is higher than the droplet generation frequency, then some of the droplets will encapsulate more than one particle (see Fig. S2d). Also, the rate of single-particle encapsulation is studied for a droplet frequency of 300 with different particle concentrations. Fig S2e shows the higher concentration yields a higher single-particle encapsulation rate.

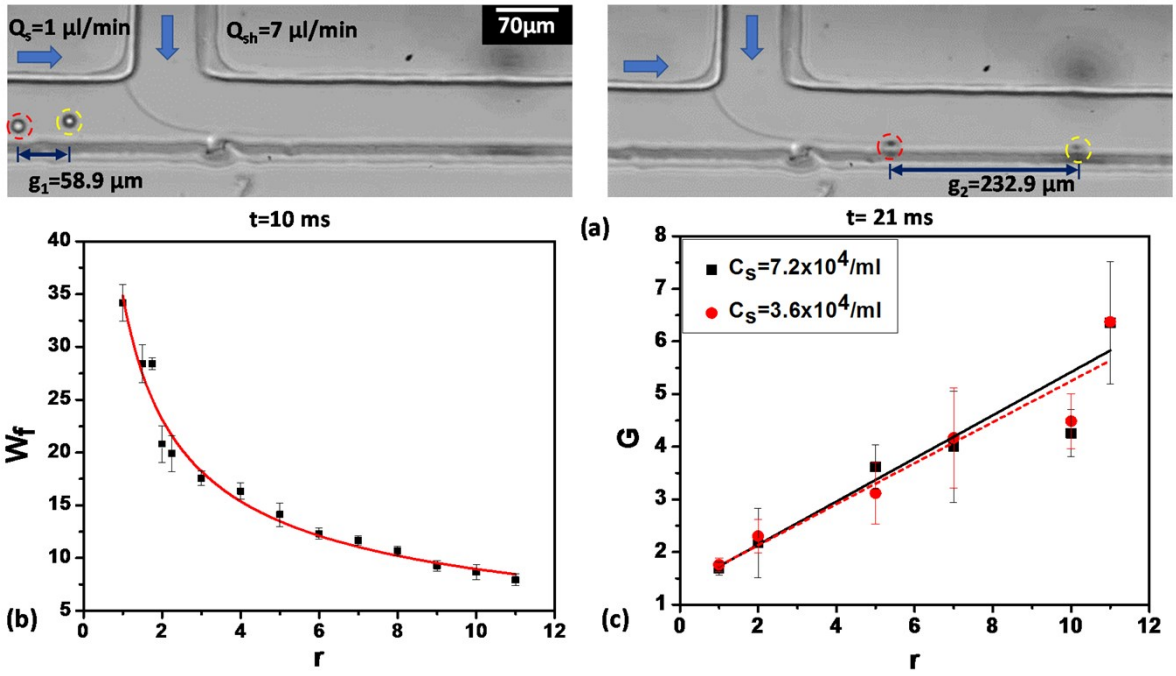

Fig. S1 (a) Experimental images of particle focusing module, (b) variation of focused width w_f with the flow rate ratio of sheath to sample fluid $r = (Q_{sh}/Q_s)$, (c) The spacing ratio of adjacent particles as a function of flow rate ratio with different sample concentration.

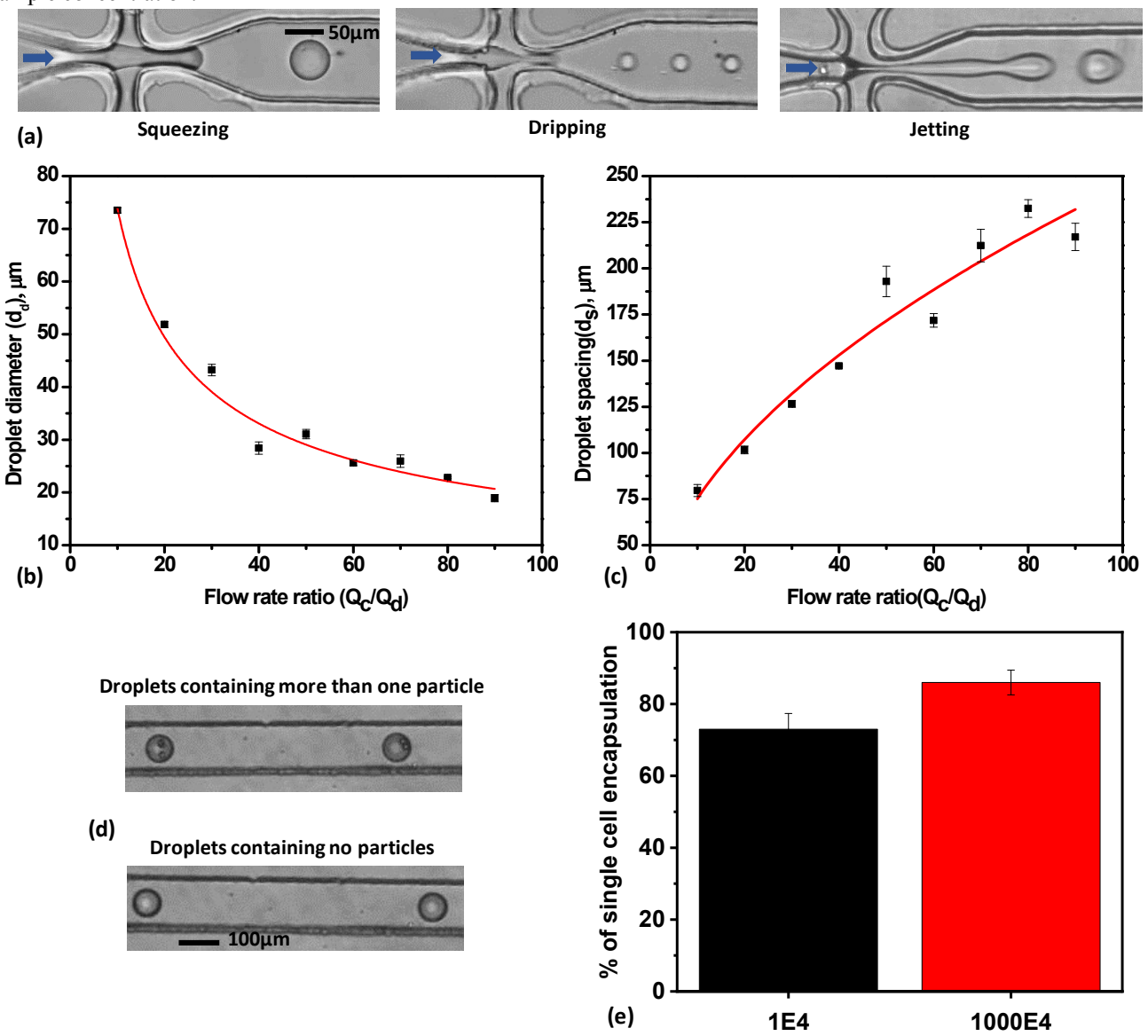

Fig. S2 (a) Experimental images showing droplet generation in a different regime, (b) variation of droplet diameter d_d with the flow rate ratio of continuous phase to discrete phase fluid $r_f = (Q_c/Q_d)$, (c) variation of droplet spacing s_d with the flow rate ratio of continuous phase to discrete phase fluid $r_f = (Q_c/Q_d)$, and (d) experimental images showing empty droplets and droplet containing two or more particles, (e) percentage of single-cell encapsulation in a droplet as a function of sample concentration (x-axis shows the concentration of cells).

S3: Numerical simulation showing droplet position inside the microchannel

We numerically analysed the droplet generation process in a microfluidic device using water as a dispersed phase and oil as a continuous phase. The simulations are carried out in a three-dimensional flow-focusing microfluidics device which is demonstrated in Fig. S3a. The dimension of inlet 1 and inlet 2 is 70µm and 100µm, whereas the dimension of the outlet channel is 100µm The dimension of the flow-focusing junction is 25 µm. The simulations are carried out using laminar two-phase flow coupling with the level set method in COMSOL 5.4.

The formulation is based on incompressible Navier-Stokes and continuity equations,

$$\rho\frac{\partial u}{\partial t} + \rho(u.\nabla)u = \nabla.\big(-pI + \mu\big(\nabla u + (\nabla u)^T\big)\big) + F_{st} \tag{1a}$$

$$\nabla.u = 0 \tag{1b}$$

where, ρ is the density, u the velocity, p the pressure, μ the viscosity and F_{st} is the surface tension force. The level set method is used to track the interface of the two-phase flow (Eqn. (2)).

$$\frac{\partial \phi}{\partial t} + u.\nabla\phi = \gamma\nabla.\left(-\frac{\phi(1-\phi)\nabla\phi}{|\nabla\phi|} + \varepsilon\nabla\phi\right) \tag{2}$$

The ϕ in the above equations denotes the level set function, and γ and ε are numerical stabilisation parameters. The Multiphysics coupling feature defines the density and viscosity according to

$$\rho = \rho_w + (\rho_o - \rho_w)\phi \qquad \mu = \mu_w + (\mu_o - \mu_w)\phi$$

where, ρ_w, ρ_o and μ_w, μ_o are the densities and viscosities of water and oil, respectively. The required fluid properties for the simulations can be found in section 2.4.

At inlet 1 and inlet 2, the laminar inflow conditions with prescribed volume flow rates $2\mu L/min$ and $5\mu L/min$ are used respectively. At the outlet, the pressure boundary condition is set. Microchannel walls are specified as wetted walls and slip length equal to the mesh size parameter, h. COMSOL physics-controlled fine mesh is used which is adequate to capture the detailed physical phenomena of the two-phase flow.

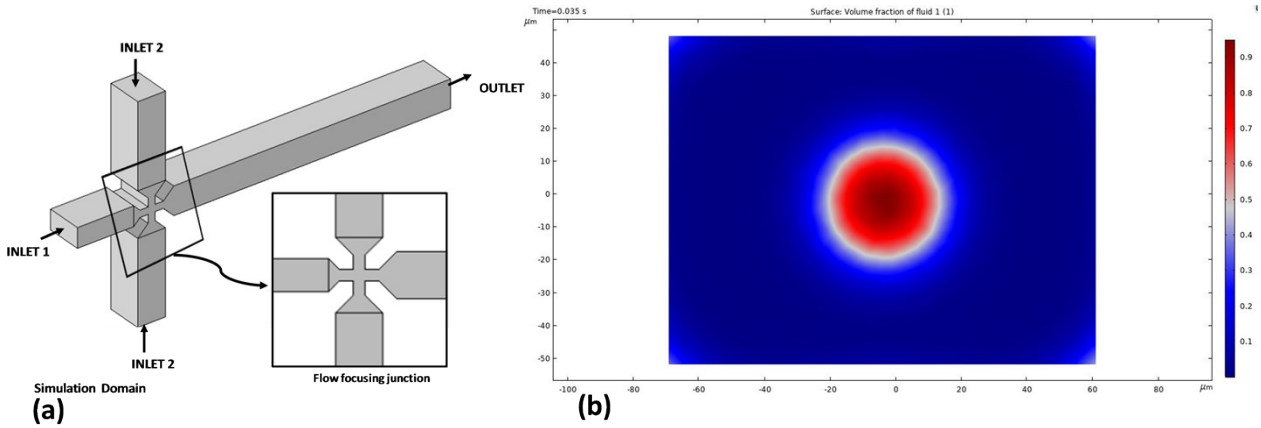

Fig. S3 (a) Schematic of the three-dimensional simulation domain, (b) COMSOL simulation results showing volume fractions of the droplet and continuous phases inside the microchannel.

S4: Optical detection of particles/cells

Fig. S4 shows the FSC, SSC and FL signals collected from the empty droplets (of size 72 µm and 60 µm), droplets containing 15 µm FL and non-FL particles.

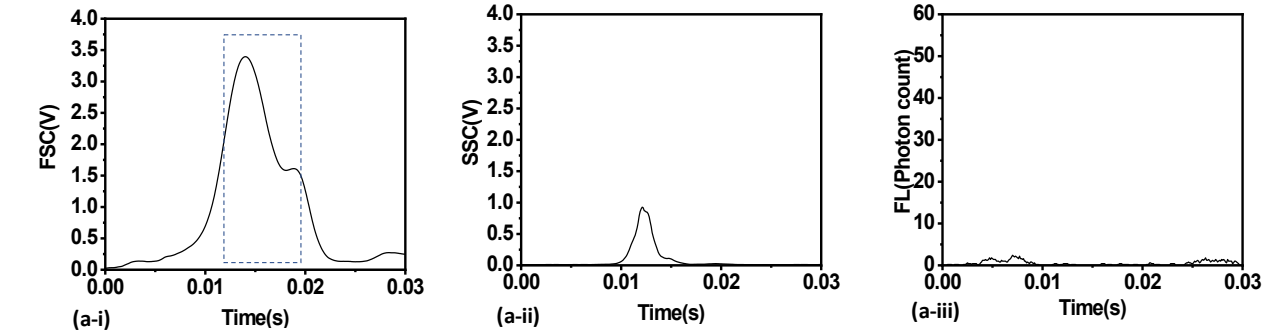

(a) FSC, SSC and FL signal from empty liquid droplets of size 68 µm.

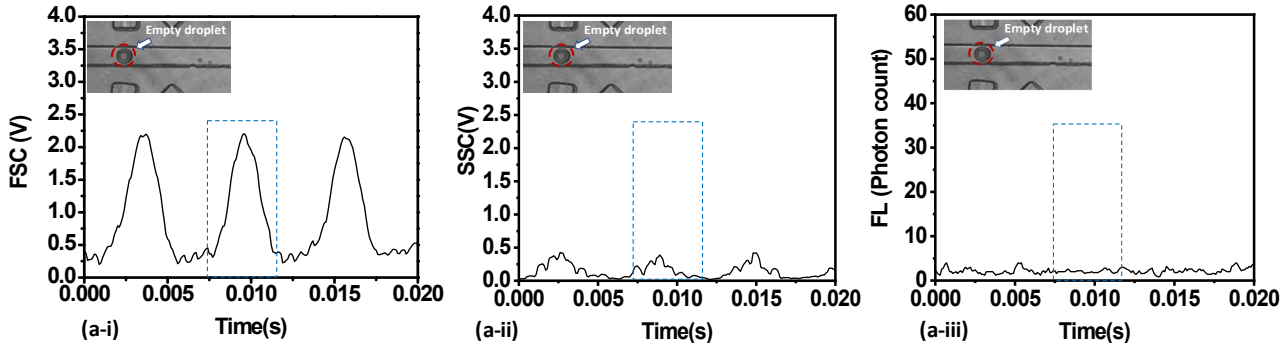

(b) FSC, SSC and FL signal from empty liquid droplets of size 60 µm.

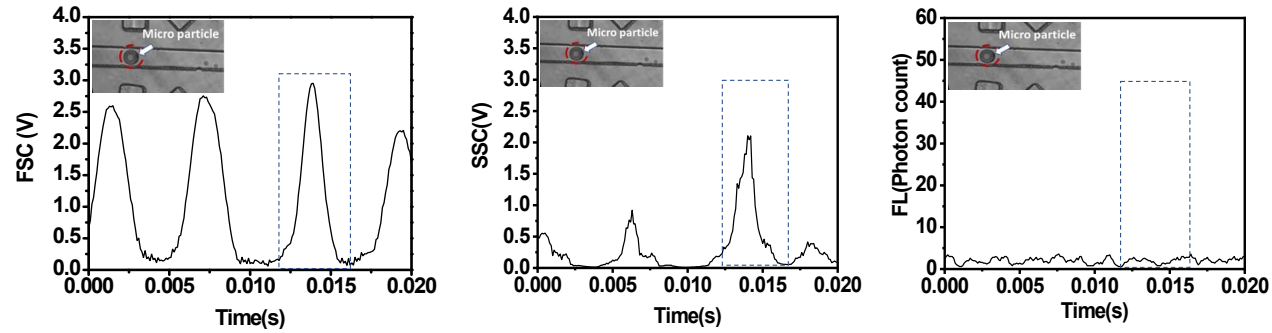

(c) FSC, SSC and FL signals of droplets of size 60 µm containing 15 µm non-FL particles.

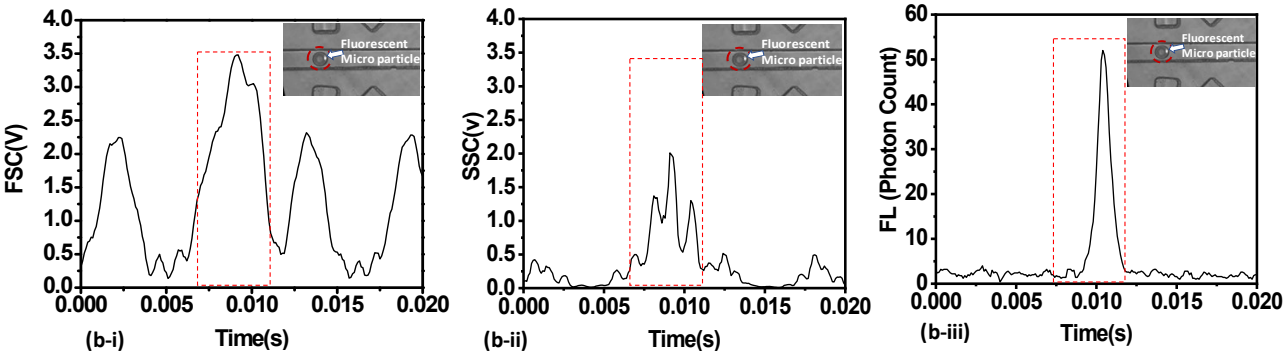

(d) FSC, SSC and FL signal from 15 µm FL microparticle encapsulated in liquid droplets of size 60 µm.

Fig. S4 FSC, SSC and FL signals collected from the empty droplets of size (a) 68 µm and (b) 60 µm, droplets containing 15 µm (c) non-FL and (d) FL particles. The FSC and SSC signals are collected with the help of avalanche photodetectors which give outputs in terms of voltage whereas the FL signal is collected using a highly sensitive detector, single-photon counting module (SPCM) which gives output in terms of the photons received. Hence, the FSC and SSC signals are represented in 'V' and FL signal in "Photon Count'.

S5: Grayscale intensity comparison

The cultured HeLa Cells are tagged with R6G and anti-Ep-CAM-FITC (protocol is discussed in section 2.4). Tagged cells are then observed under the microscope and fluorescence images are captured with the help of a colour camera. Captured images are then converted to grayscale using a MATLAB programming (See Fig. S8). The Fig a and b show the greyscale intensities across the cell tagged with R6G and anti-Ep-CAM-FITC antibody, respectively

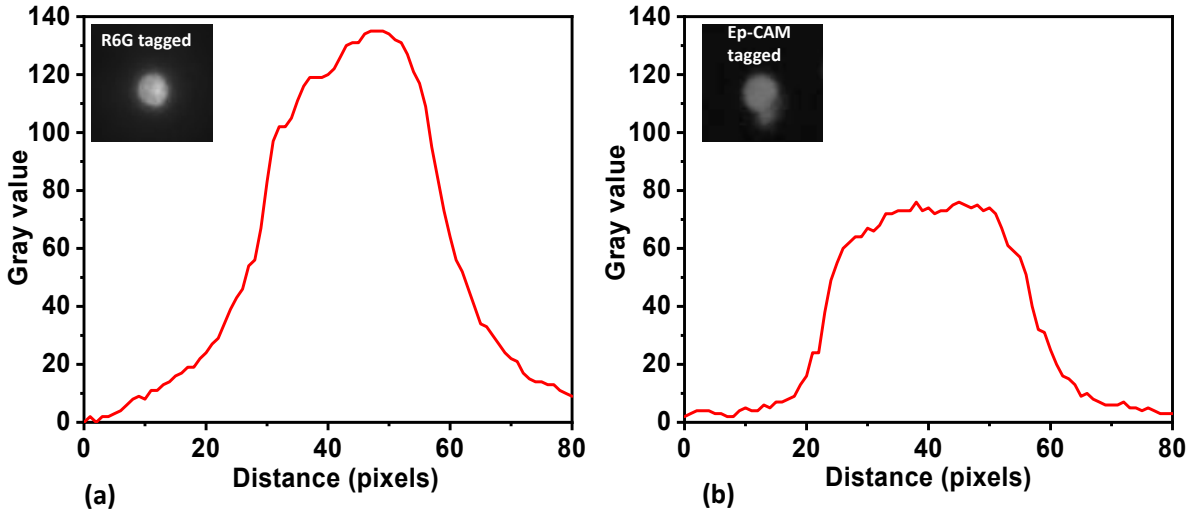

Fig. S5 Grayscale intensities across the FL images of the cells tagged with (a) R6G and (b) anti-Ep-CAM-FITC.

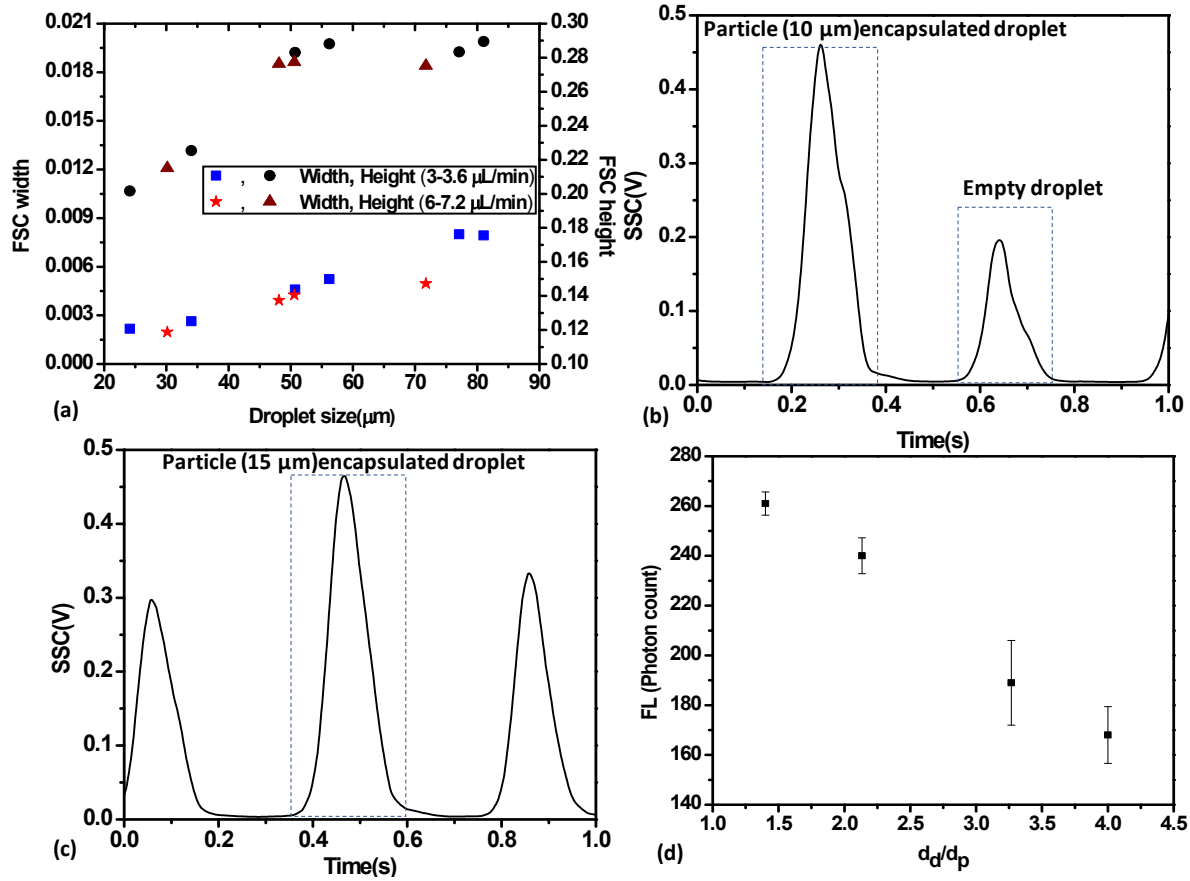

Fig. S6 (a) variation of FSC signal parameters such as height and width as a function of droplet size, (b) SSC signal for empty droplet and droplet containing particle (10µm), and (c) SSC signal for a droplet containing 15µm particle, (d) FL signal intensity as a function of droplet diameter to particle diameter ratio $\left(d_d/d_p\right)$.

S5: Electro coalescence of droplets

Fig. S6a shows the time evolution of coalescence of all empty droplets as well as droplets containing microbeads of 15 µm size. The variation in the width of the oil stream with the oil-to-aqueous stream flow rate ratio is depicted in Fig. S6b. The effect of the size and velocity of the droplets on the electric field required for coalescence was studied (see Fig. S6c and S6d).

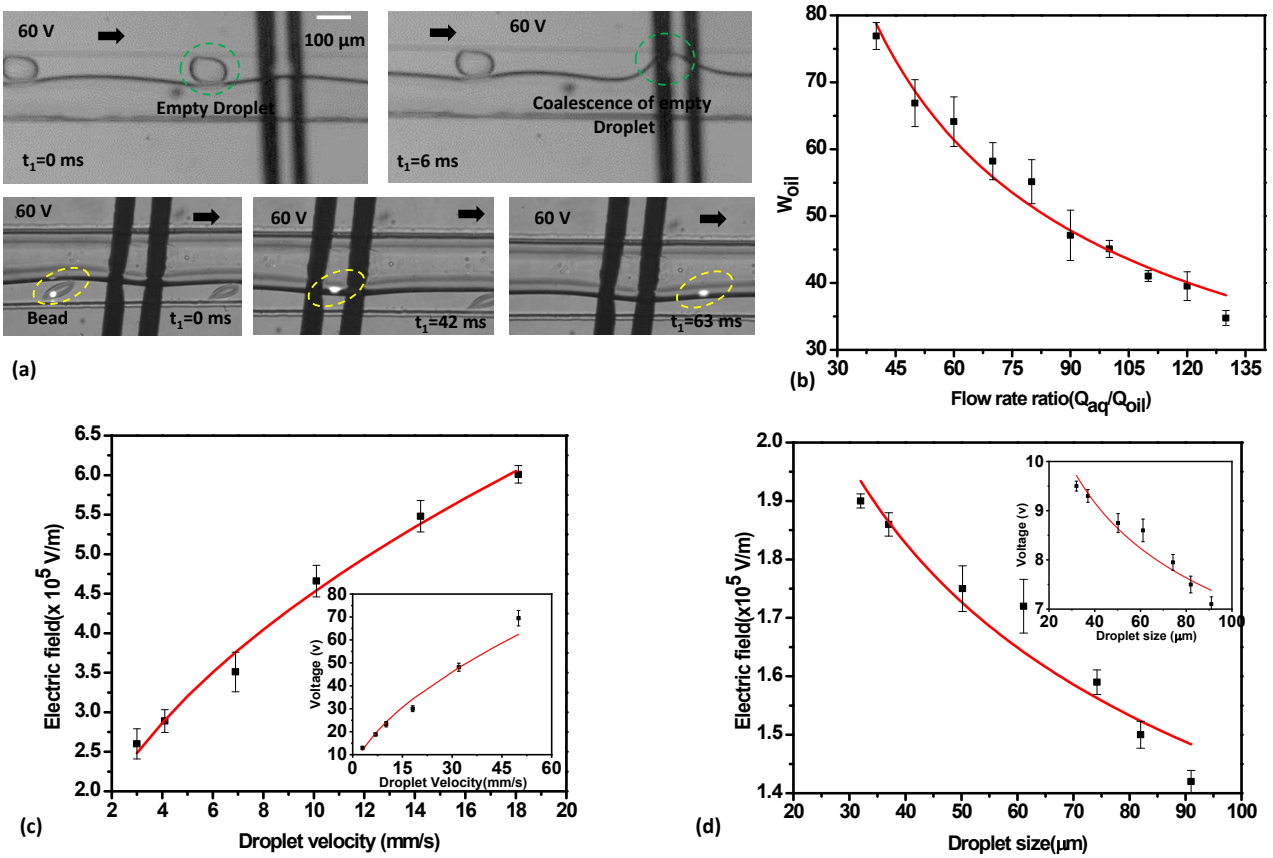

Fig. S7 (a) Experimental images showing coalescence of empty droplets and droplets containing fluorescent particles, (b) oil phase width variation with the ratio of flow rates of aqueous phase to the oil phase $r_s = (Q_{aq}/Q_{oil})$ and (c) electric field required for the coalescence as a function of droplet velocity and droplet size, corresponding voltages are shown as insets.

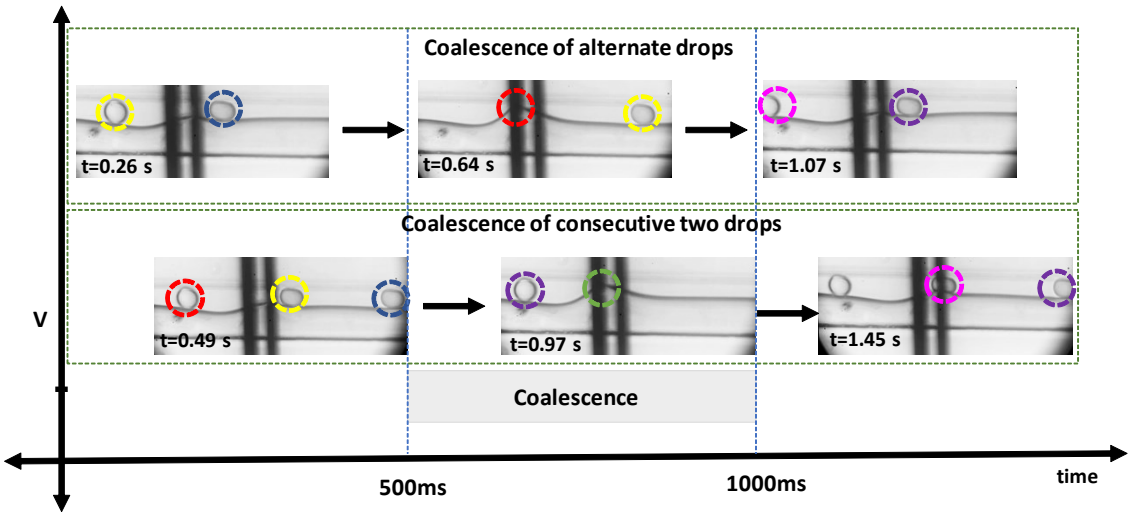

Fig. S8 Coalescence of droplets in a specific sequence: alternate and two consecutive droplets.

Table S1 Performance parameters for the positive sorting experiments.

	Initial Conc.	Enrichment	Efficiency (%)	Recovery (%)	Purity (%)
Florescent	3.3×10^4	3200X	99.04	91.21	99.08
Non-florescent	10^6				
HeLa	2.4×10^3	1600X	98.79	98.87	98.38
PBMC	6.4×10^5				
DU145	2.9×10^4	2400X	98.21	98.96	96.60
PBMC	10^6				

S6: Cell viability measurements

Cell suspension of volume 10 µL taken in an Eppendorf tube was mixed with 10 µL of 0.4% trypan blue (Sigma-Aldrich). The mixture was then allowed to incubate for 3 min at room temperature (25 °C). A 10 µL trypan blue/cell mixture was gently applied to the hemocytometer chamber placed on the stage of the inverted microscope. The cells were observed through the eyepiece using a 10X objective lens and counted using a hand tally counter. The number of live and dead cells in the four corner squares and the middle square of the hemocytometer were counted for determining the % cell viability as follows,

$$\%\ Cell\ viablity = \frac{Live\ cells}{(Live\ cells + Dead\ cells)} \times 100$$

The cell counting was performed within 5 min of incubating with trypan blue since longer incubation may lead to cell viability. The following tables summarise the counting data for the number of live and dead cells for each of the three different cases, i.e. the unsorted case, the sorted case with positive and negative sorting techniques (with two trials for each case, and HeLa cells), and the % cell viability.

Negative Sorting:

Trial-1

	Top Left	Top right	Middle	Bottom left	Bottom right	Total	%cell viability
Live Cells	89	70	81	76	83	399	94.32
Dead Cells	5	3	1	2	13	24	

Trial-2

	Top Left	Top right	Middle	Bottom left	Bottom right	Total	%cell viability
Live Cells	82	75	88	72	87	404	95.05
Dead Cells	3	5	4	5	4	21	

Positive Sorting:

Trial-1

	Top Left	Top right	Middle	Bottom left	Bottom right	Total	%cell viability

Live Cells	81	41	75	79	69	345	96.91
Dead Cells	2	2	1	5	1	11	

Trial-2

	Top Left	Top right	Middle	Bottom left	Bottom right	Total	%cell viability
Live Cells	70	72	69	72	65	348	97.20
Dead Cells	1	3	2	1	3	10	

Unsorted:

Trial-1

	Top Left	Top right	Middle	Down left	Bottom right	Total	%cell viability
Live Cells	68	60	72	71	45	316	98.75
Dead Cells	1	0	1	1	1	4	

Trial-2

	Top Left	Top right	Middle	Down left	Bottom right	Total	%cell viability
Live Cells	65	64	67	62	63	321	99.07
Dead Cells	1	0	1	0	1	3	

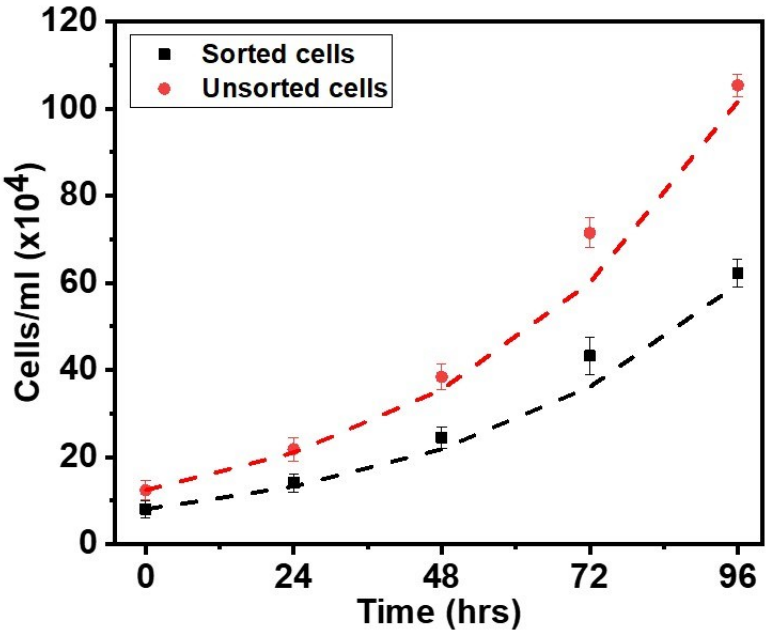

Fig. S9 Variation of the concentration of cells per ml of the suspension (c) is plotted with time (t, in hrs) for both sorted and unsorted case. The dotted lines show the correlation between time and concentration ($c = A\,K^{0.05t}$, where $A = 8.2 \times 10^4$, $K = 1.52$ for sorted cells and $A = 12.4 \times 10^4$, $K = 1.54$ for unsorted cells).

References

(1) Jayaprakash, K. S.; Sen, A. K. Droplet Encapsulation of Particles in Different Regimes and Sorting of Particle-Encapsulating-Droplets from Empty Droplets. *Biomicrofluidics* **2019**, *13* (3). https://doi.org/10.1063/1.5096937.

(2) Hazra, S.; Jayaprakash, K. S.; Pandian, K.; Raj, A.; Mitra, S. K.; Sen, A. K. Non-Inertial Lift Induced Migration for Label-Free Sorting of Cells in a Co-Flowing Aqueous Two-Phase System. *Analyst* **2019**, *144* (8), 2574–2583. https://doi.org/10.1039/C8AN02267D.